Hindawi
Shock and Vibration
Volume 2019, Article ID 4678491, 10 pages
https://doi.org/10.1155/2019/4678491

Research Article

Bearing Fault Diagnosis Based on Spatial Features of 2.5 Dimensional Sound Field

Junjian Hou,[1,2] **Jun Ma**,[1,2] **Zhanpeng Fang**,[1,2] **Wuyi Ming**,[1,2] **and Wenbin He**[1,2]

[1]*Mechanical and Electrical Engineering Institute, Zhengzhou University of Light Industry, Zhengzhou 450002, China*
[2]*Henan Key Laboratory of Mechanical Equipment Intelligent Manufacturing, Zhengzhou 450002, China*

Correspondence should be addressed to Junjian Hou; houjunjian@zzuli.edu.cn

Received 4 October 2018; Revised 25 December 2018; Accepted 9 January 2019; Published 14 February 2019

Academic Editor: Paola Forte

The traditional acoustic-based diagnosis (ABD) technique based on single-channel testing has a significant engineering value. Since its diagnosis robustness is sensitive to sound signal acquisition location, it develops slowly. To solve this problem, the 2-dimensional (2D) sound field variation near the machine is adopted for diagnosis by the near-field acoustic holography (NAH)-based fault diagnosis method with array measurement. However, its performance is limited due to the neglect of the sound field normal change information. To dig the sound field fault information further, a 2.5-dimensional (2.5D) acoustic field diagnosis method is presented in this paper and its performance compared with the 2D technology is verified by the bearing diagnostic test. Different from the 2D technique with only one source image, the 2.5D acoustic field model consists of source image, holographic sound image, and the differences between them, and its effective feature model is constructed by Gabor wavelet feature extraction and random forest feature reduction algorithm. The diagnostic effect of the 2.5D technique compared with the 2D technique increases more than 11% in the bearing diagnostic test. It provides new ideas for the development of the NAH-based fault diagnosis method, and further improves the ABD technique-based array measurement.

1. Introduction

Fault diagnosis has great significance to support equipment for safe and reliable operation and reduce maintenance costs. When a machine works, mechanical vibration will occur by the dynamic forces within the machine. This vibration pattern changes when an initial fault starts to evolve. The vibration signals can be easily detected by different kinds of sensors mounted directly onto the machine, such as position sensors, velocity sensors, and accelerometers. Thus, vibration-based fault diagnosis has been a well-established field for the last decades, and many vibration signal analysis techniques have rapidly developed—time analysis [1, 2], frequency and Cepstral analysis [3–5], time-frequency analysis [6–8], nonlinear in time [9, 10], and so on. However, since the vibration sensor needs to be placed on the fault sensitive part of the equipment, it can capture the vibration signal with better signal and noise, which limits the application of vibration analysis technology in high temperature, humidity, and dangerous conditions.

As another expression of mechanical energy transmission, the sound signature also carries information about the condition of the machine. Therefore, extracting the acoustic characteristics of the machine to detect failure parts is an effective technique in fault diagnosis [11, 12]. Acoustic emission (AE) technique uses the transient elastic wave caused by the release of energy stored in the material under stress to identify the fault. It has the advantage of incipient defect identification in comparison with vibration-based diagnosis technique [12]. However, to collect the AE signals with the frequency range 100 kHz–1 MHz in practice, the special piezoelectric sensors, the advanced signal processing techniques, and the data analysis techniques are required, which partially limit the wide application of the AE technique [13]. The conventional ABD technique usually adopts the microphones which are not in contact with the device to collect acoustic signals near the machine. The noncontact measurement, simple operation, and not affecting the normal operation of the equipment are the advantages of the ABD technique, and the sound signals can

also be processed by the vibration signal analysis technology. As the input features, the time-domain statistical features and frequency-domain energy features of the acoustic signals are adopted to diagnose the mass unbalance faults effectively [14]. In particular, the usage of Hilbert envelope analysis in the vacuum cleaner production detection [15] and the spectral entropy in diagnosing the cavitation of the centrifugal pump [16] are successful, in which the acoustic-based analysis gets better results than the vibration signals. However, compared with the vibration-based diagnosis technology, the traditional ABD technology is developing slowly since the audio signals are sensitive to environmental noise [11]. To obtain the effective signals with high signal-to-noise ratio, the choice of measurement positions of microphones should be seriously considered [17]. A NAH-based fault diagnosis technique with the microphone array test is presented to improve the problem, which adopts the two-dimensional sound field variation near the machine for fault detection [18–20]. Different from the previous signal analysis procedure in traditional ABD technology, the two-dimensional acoustic pressure distribution near the sound source of the machine is implemented according to the program of image recognition and classification, which is obtained by the array test and NAH-imaging algorithm. This provides a new idea for ABD technique and has proven effectively in bearing fault diagnosis. Although the method which regards amplitude distribution of sound pressure on bearing sound source surface as the object transforms the fault diagnosis problem into the image pattern recognition innovatively, there is a problem of ignoring the variation of sound pressure in normal direction of the sound field. The insufficient description of sound field can limit the diagnostic effects under various working conditions, especially in the weak fault condition where the local acoustic pressure amplitude changes little.

In view of the above problems, a new 2.5D sound field diagnosis technology is proposed and employed to diagnose bearing failure in this paper. It coopts the construction thoughts of the 2.5D underground tunnels seismic analysis model [21, 22] and the frame difference theory in video-processing technique [23, 24] and builds a 2.5D sound field model to describe the characteristics of sound field more well. Sound field is a spatial field with three dimensions. The 2D acoustic image diagnosis technology, using one plane sound field near the sound source, ignores the acoustic wave transmission change in the normal direction of sound field. But, it is unrealistic to consider the continuous change of normal space in engineering completely. The 2.5D sound field spatial model put forward in this paper is between two-dimensional sound field and three-dimensional sound field, which is composed of two-dimensional sound field distribution at the location of sound source, two-dimensional sound field distribution at the location of the normal holographic measurement of sound field, and variation of the difference of normal sound pressure transmission at each node of the 2 two-dimensional plane sound fields. The two-dimensional sound field distribution at the normal holographic measurement position is the result of the common radiation and interaction of each bearing sound source. Compared with the two-dimensional sound field at the sound source position, it represents the evolution information of sound source after transmitting a certain distance and contains the normal change information of sound field. At the same time, the sound pressure difference of the two-dimensional sound field at the holographic measurement position and the sound source position can weaken the influence on the interference source and background noise and highlight the state change information of the sound source.

The bearing acoustic signals are measured through holographic array, and the amplitude distribution of sound pressure of the two-dimensional acoustic field at the holographic measurement position can be directly obtained. Meanwhile, NAH technology is applied to reconstruct the two-dimensional sound field information at the bearing sound source location. Then, a 2.5D sound field model with the information of normal spatial change is constructed, which is made up of source image, holographic sound image, and the difference between them. Its changed characteristics are described by the Gabor wavelet features. In addition, based on the random forest feature selection algorithm, certain valuable Gabor wavelet features are closely related to the running state of the bearing are selected. And then, the support vector machine is used for pattern classification to realize the bearing fault diagnosis. Compared with acoustic image diagnosis technology, the 2.5D acoustic field fault diagnosis technology improves the diagnosis robustness by further integrating the sound field change information of the normal dimension and further develops the ABD technology based on the array test and acoustic imaging algorithm.

2. Fault Diagnosis Based on 2.5D Sound Field

2.1. Technique Flow. The diagnosis process based on the spatial features of the 2.5D sound field is shown in Figure 1. First, array test technology is used to collect sound field information of sample machinery and machinery to be diagnosed. The spectrum analysis of the sample audio signals of the microphones near the reference sources is carried out. For a certain kind of fault, the amplitudes of the fundamental frequency and its octave frequencies are compared and analyzed. Within the limited frequency range of NAH imaging accuracy, the frequency with variable amplitude and higher amplitude among its sidebands is defined as the fault-sensitive frequency. Based on the fault-sensitive frequency, the NAH image algorithm is used to reconstruct the sound pressure distribution on the surface of the sound source in sample and test machinery. And, the sound pressure amplitude under the fault frequency at each node of the holographic measurement array is directly extracted. The amplitude distribution of sound pressure at the holographic measuring position is obtained. Different from the 2D technique using the source image only, the sound field model of 2.5D technique is built together with the source image, the holographic sound image, and the difference between them. Then, Gabor wavelet features are extracted from the 2.5D sound field, the random forest algorithm is applied for feature dimension reduction, and an effective 2.5D sound field feature model is built. Finally, support vector machine is adopted to train the samples to get the best classifier parameters, and the test machinery is diagnosed by the optimal classifier.

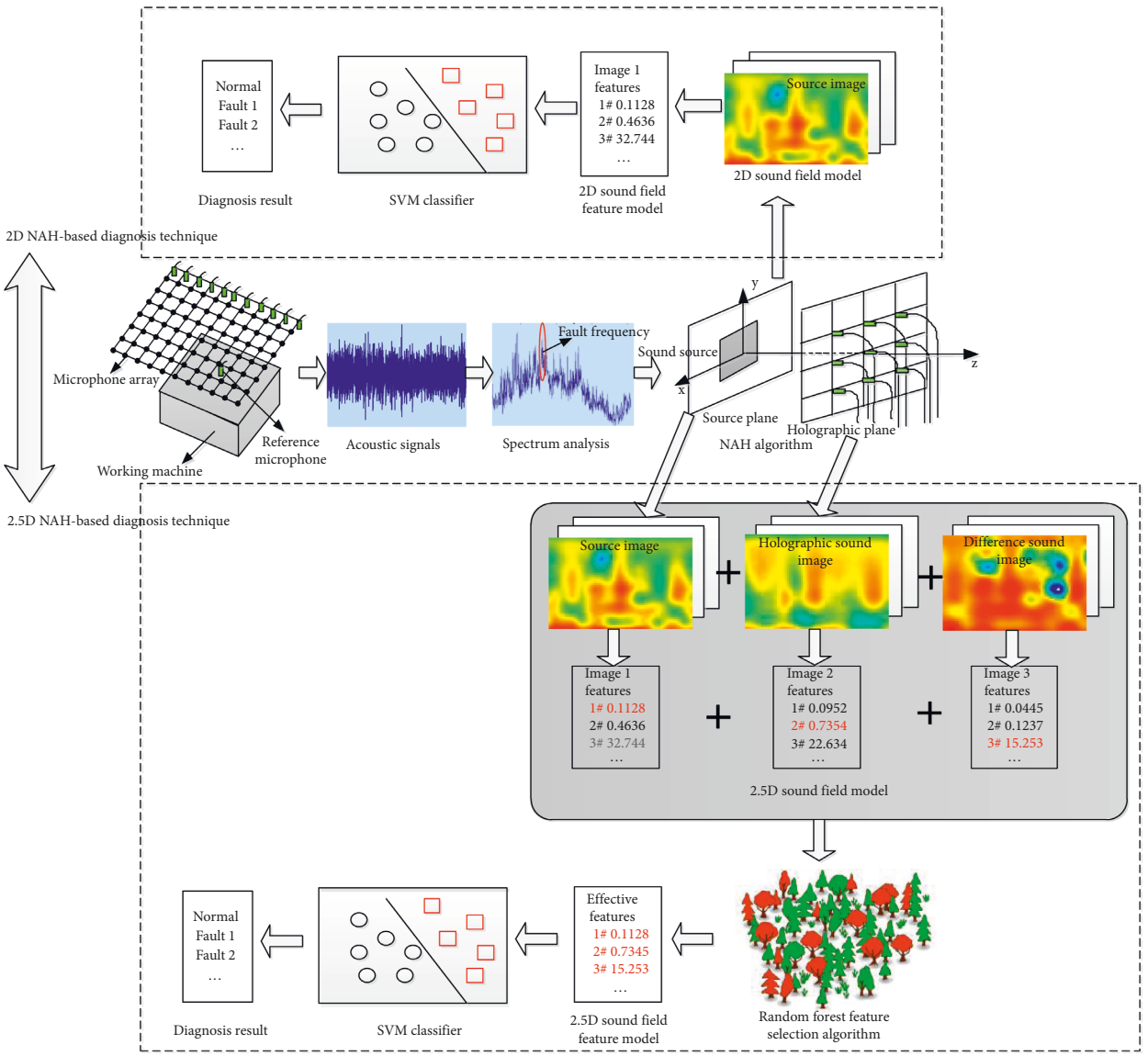

Figure 1: Flowchart of fault diagnosis based on 2D/2.5D sound field.

Compared with the 2D acoustic image fault diagnosis procedure, the main improvements of the 2.5D acoustic field diagnosis technique are as follows:

(1) Construction of 2.5D acoustic field model: after the array measurement of the sound signals, spectrum analysis of every microphone is implemented and the acoustic pressure amplitude at the fault sensitive frequency is picked up to form the holographic sound image. Then, the NAH imaging algorithm is carried out to reconstruct the sound source image. The source image is subtracted from the holographic sound image to obtain the difference sound image, which describes the normal variation of sound field between the sound source and the array measurement position. Finally, the 2.5D acoustic field model containing spatial change information is constructed by synthesizing the three acoustic images.

(2) Effective features of 2.5D acoustic field: firstly, extract Gabor wavelet features of three acoustic images in the 2.5D acoustic field model and arrange them in order to preliminarily construct the eigenvector. Secondly, the importance of eigenvector is analyzed by using the random forest algorithm. Finally, an effective eigenvector is further constructed based on the significance effect of features on the classification results and the diagnostic efficiency.

Based on the idea of information fusion, the new ABD technology with the 2.5D sound field model enriches the sound field normal change information, whilst the random forest dimension reduction technology is adopted to retain effective information and remove redundant information, which can further improve the robustness of the diagnosis.

2.2. Sound Field Reconstruction by NAH. NAH is a hot technique in visualizing sound field and can reconstruct the mechanical sound field accurately. It collects sound pressure on the holographic-measuring surface surrounding the sound source and rebuilds the sound field on the sound source surface by means of the spatial field transformation relationship between the sound source surface and the holographic surface [25]. Typical imaging principles are shown in Figure 2.

FFT-based NAH is a simple frequency-domain sound field reconstruction technology and is implemented in this paper. Assume the holographic plane S_h is located at $z = z_h$, the reconstruction plane S_c is located at $z = z_c$, and the sound source surface S_s is located at $z = z_s$. The sound pressure on S_h and S_c is, respectively, $\varphi(x, y, z_h, f)$ and $\varphi(x, y, z_c, f)$, and f is the reconstruction frequency. Given Green's function $G_D(x, y, z_h - z_c, f)$ satisfying Dirichlet boundary conditions, the generalized reconstruction formula can be obtained [21]:

$$\begin{aligned}\varphi(x, y, z_c, f) &= F^{-1}\left[\widetilde{\varphi}\left(k_x, k_y, z_h, f\right)\right. \\ &\quad \left.\cdot\, \widetilde{G}_D^{-1}\left(k_x, k_y, z_h - z_c, f\right)\right], \\ \widetilde{\varphi}\left(k_x, k_y, z_h, f\right) &= F[\varphi(x, y, z_h, f)], \\ \widetilde{\varphi}\left(k_x, k_y, z_c, f\right) &= F[\varphi(x, y, z_c, f)], \\ \widetilde{G}_D\left(k_x, k_y, z_h - z_c, f\right) &= F[G_D(x, y, z_h - z_c, f)].\end{aligned} \tag{1}$$

In the formula, F denotes the two-dimensional FFT, and the superscript -1 means the inverse transformation; k_x and k_y are the spatial wavenumbers along the x and y directions, respectively.

2.3. Gabor Wavelet Feature Extraction. The texture information of the image can reflect the local subtle changes of the image effectively, and the diagnostic robustness of Gabor wavelet feature is verified [26, 27] effectively. Therefore, Gabor wavelet feature is also employed in this paper to describe the sound field changes.

Assume $f(x, y)$ is used to denote the image with size $M \times N$; then, the two-dimensional discrete Gabor wavelet of the image is changed into

$$I_{p,q}(x, y) = \sum_s \sum_t f(x - s, y - t)\varphi^*_{p,q}(s, t). \tag{2}$$

In this formula, s and t denote the variables of the filter mask size, x and y are the locations of pixels in the image, p and q represent the scale and direction of wavelet transformation, respectively, and $\varphi_{p,q}$ is the Gabor wavelet transformation function.

The texture classification features of the image usually adopt mean value $\mu(p, q)$ and standard deviation $\sigma(p, q)$:

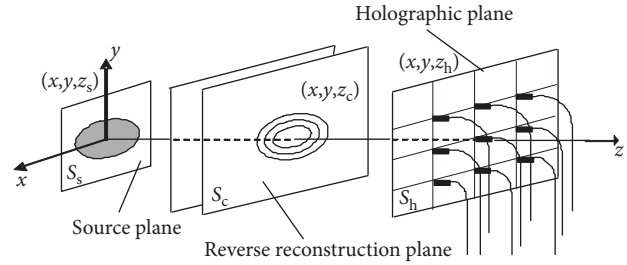

Figure 2: Sketch map of sound field propagation [19].

$$\begin{aligned}\mu(p, q) &= \frac{E(p, q)}{MN}, \\ \sigma(p, q) &= \sqrt{\frac{\sum_x \sum_y \left(\left|I_{p,q}(x, y)\right| - \mu(p, q)\right)^2}{MN}}.\end{aligned} \tag{3}$$

In this paper, the common values 5 and 8 are, respectively, taken for p and q [28], and the extracted Gabor wavelet feature eigenvector is expressed as follows:

$$\textbf{Gabor} = \left[\mu_{0,0}, \sigma_{0,0}, \mu_{00,1}\sigma_{00,1}, \ldots, \mu_{P-1,Q-1}, \sigma_{P-1,Q-1}\right]. \tag{4}$$

2.4. Feature Dimension Reduction of Random Forest. Random forest is a new machine learning method which is composed of multiple classification and regression tree (CART) and decision trees. N sample sets are selected by putting back from the original training sample set through bootstrap resampling technique repeatedly and randomly, and the number of samples taken every time accounts for about 2/3 of the original sample set. Then, N CART decision trees are generated based on the new training set, and a new random forest model is constructed. In the growth process of every tree, the optimal attribute is selected for internal node branches based on the principle of minimum Gini coefficient. Finally, N tree voting results are collected to classify the new samples [29].

About 1/3 of the data which were unselected in every sampling are called out of bag (OOB). The importance of feature variables $V(X_j)$ can be obtained by using OOB internal error estimation:

$$V\left(X_j\right) = \frac{1}{N}\sum_{i=1}^{N}\left(e_i^j - e_i\right). \tag{5}$$

In the formula, e_i is the OOB error of the number i decision tree, X_j is the number j characteristic variable of OOB data, and e_i^j is the new OOB error after changing the X_j size randomly. The larger the OOB error caused by the change of X_j, the more the accuracy is reduced, indicating the variable is more important.

2.5. Pattern Classification by SVM. SVM is a high-performance machine learning method based on structural risk minimization principle and statistical learning theory, which has been widely used in the field of pattern

recognition. The key thought is to seek an optimal classification hyperplane to meet the classification requirements. Assume n samples are represented as $\{x_i, y_i\}_{i=1}^{n}$, $i = 1, 2, \ldots, n$, $x_i \in R_n$ as training sample input for n dimension, and $y_i \in R_n$ as the training sample output; then, the problem of establishing linear SVM can be converted into solving a convex quadratic programming problem [30]:

$$\begin{cases} \min\limits_{w,b,e} J(\mathbf{w}, \zeta_i) = \dfrac{1}{2}\mathbf{w}^{\mathrm{T}}\mathbf{w} + C\sum\limits_{i=1}^{n}\zeta_i, \\ \text{s.t. } y_i\left[\mathbf{w}^{\mathrm{T}}\varphi(x_i) + b\right] = 1 - \zeta_i, \ \forall i. \end{cases} \tag{6}$$

In the formula, φ denotes kernel space mapping function; $\mathbf{w}$ is the weight vector; b is the bias term; ζ_i is the error variable, namely, the relaxation factor, which represents the coefficient that allows a certain degree of wrong classification; and C is the penalty coefficient, which is used to compromise between the minimum error sample and the maximum classification interval.

In the identification process, the sample set is randomly sequenced for 5 times, and 3/4 of every random sorted sample is taken as the training sample and the remaining 1/4 is used as the test sample to build a 5 duplicate cross-validation sample database, and the average value of the five-time identification rate is picked up as the final recognition effect.

3. Bearing Fault Diagnosis Test

3.1. Establishment of the Test Bench. Bearing is one of the most common vulnerable and important parts of mechanical equipment; its running state affects the whole mechanical performance directly. The diagnosis of bearing state has an important engineering value. Therefore, bearing fault diagnosis has always been a research hotspot in the field of fault diagnosis. By selecting bearing as the research object, verifying the effectiveness of the new 2.5D ABD technique and its advantages over the 2D acoustic image diagnosis technology has better universality and higher engineering practical value.

In order to ensure the repeatability of the test and reduce the influence on the repeated disassembling of the parts in the test system on research results, the machinery fault simulator (MFS) test bench manufactured by SpectraQuest Inc. of the United States is adopted. At the same time, the test bench is modified based on the idea of improving signal-to-noise ratio (SNR) of the bearing and keeping load constant, and the motor bearing test bench is built. The arrangement of the motor bearing test bench and the relative position of every part are shown in Figure 3, which is mainly composed of the motor, coupling, transmission shaft, bearing, and rotor. The test bench is driven by a 1 hp motor at a constant speed of 120 rpm. The rotor is driven by the coupling and transmission shaft. Transmission shaft is supported by two bearings of the same type on both sides. The inner ring of the bearing rotates synchronously with the transmission shaft. The transmission shaft is 1 inch in diameter; the rotor model is M-BL-1, with a mass of 5 kg and a rotating inertia of 0.015 kg·m^2. The bearing has been selected as a removable ER-16K that can be matched with the transmission shaft. The rotor with a large moment of inertia and mass can be assumed to have a constant load, and the relative position of the two bearings remains unchanged throughout the test.

The bearing test system is shown in Figure 4, which mainly adopts microphone linear array scanning technology. To obtain high SNR sound signals further, the test is carried out in one capacious plant similar to the free sound field in which the background noise and reflection interference are controllable and negligible. Based on the comprehensive consideration of the fault frequency range and the size of the test bench and the reconstruction precision of near-field acoustic holography, the size of the holographic measuring plane is set as 0.45 m × 1.8 m, namely, the area surrounded by dotted line in Figure 3. In the direction of the width of the holographic surface, the microphone array spacing is set at 0.05 m and 10 microphones are arranged. In the direction of the length of the holographic surface, the scanning step length is set to 0.05 m, a total of 37 steps, and the measuring points of the holographic surface are 10 × 37. The distance between the holographic measuring plane and the highest point of the test bench—the top distance of the motor—Z is 0.05 m. Since the noise signals were measured by scanning steps of linear array, the scanning technology are asynchronous, and the reference source microphones shall be arranged near the main sound source positions of motor, bearing 1 and bearing 2 to retain phase information. LMS SCADAS Mobile, a data acquisition system of 16 channels, is used to synchronously collect the acoustic signals of each channel. The band range of the frequency of the microphones is 20 Hz–20 kHz, which are manufactured by BSWA Technology Co., Ltd., China. The sampling frequency is 4096 Hz, and 5 s is collected at each step.

3.2. Working Condition Settings and Sensitive Frequency Determination. In most cases, it is a gradual process for the bearing from the normal to failure, and the bearing state change of certain key components will affect the performance of the whole equipment. Based on the motor-bearing test system, bearing 1 close to the motor is assumed to be nonkey monitoring bearing, while bearing 2 far from the motor is assumed to be the key bearing under monitoring. The bearing inner ring is selected as the research object during the test, and different running states of the bearing inner ring are simulated by machining holes of different diameters in the bearing inner ring with the electric discharge machining (EDM) method, as is shown in Figure 5.

The system is in fault state when the failure diameter of bearing 2 inner ring hole is set as $\varphi_2 > 0.5$ mm. When $\varphi_2 < 0.5$ mm, the system is in normal state. Bearing 1 is only used as the source of interference. During the test sampling, (1) normal state: $\varphi_1 \in [0, 1.2]$ in bearing 1 and $\varphi_2 \in \{0, 0.4\}$ in bearing 2, a total of 36 groups are sampled; (2) failure state: $\varphi_1 \in [0, 1.2]$ in bearing 1 and $\varphi_2 = 0.6$ mm in bearing 2, a total of 36 groups are sampled.

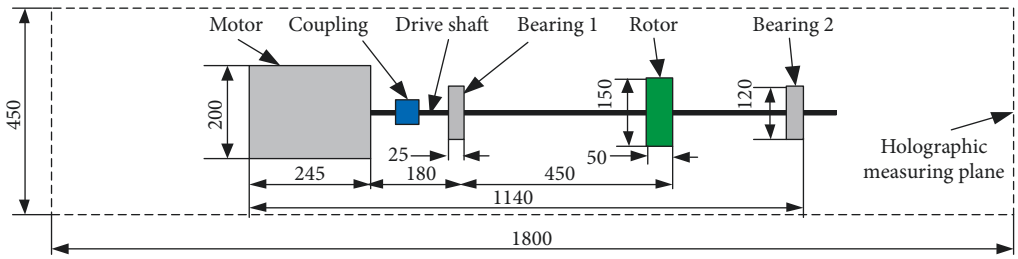

Figure 3: Layout diagram of the motor-bearing system.

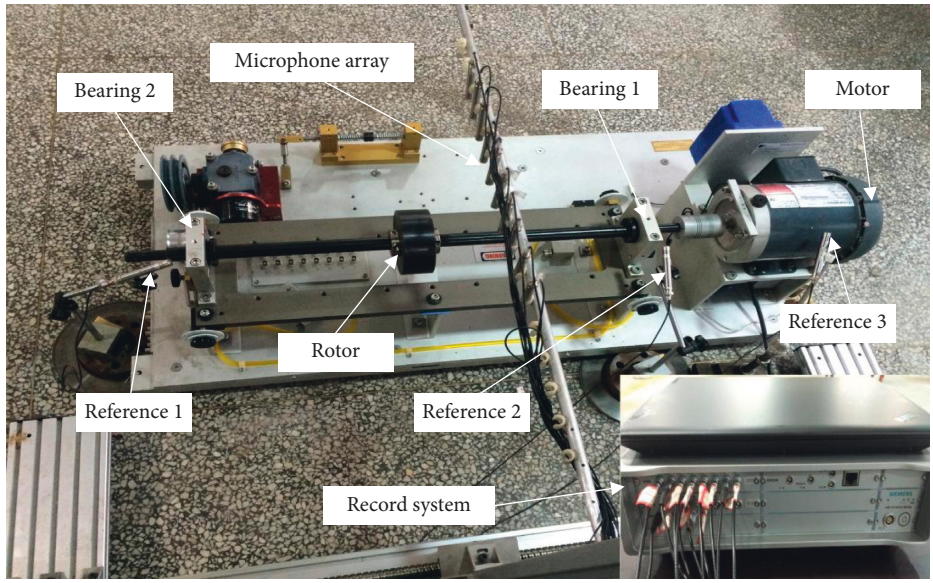

Figure 4: Bearing test rig.

Figure 5: Bearing inner-race fault by EDM.

Based on the structural parameters of the test bearing ER-16K and the rotational speed of the drive shaft, the bearing inner ring fault frequency in theory is $f_i = 107.4$ Hz and its octaves. The acoustic signal of the reference source 3 near the key bearing 2 is analyzed in the fault condition, as shown in Figure 6. When the frequency resolution is 2 Hz, the theoretical fault fundamental frequency f_i is not significantly reflected, while the peak of $4f_i$ 429.6 Hz (430 Hz in Figure 6) f_i 859.2 Hz (860 Hz in Figure 6) are relatively convex. Different from the frequency spectrum with more high amplitude near the $4f_i$, the amplitude at the $8f_i$ has obvious advantages in the spectrum near it. To obtain better signal-to-noise ratio, the $8f_i$ (859.2 Hz) is selected as the fault sensitive frequency of the motor-bearing system.

3.3. Test Results and Analysis. Based on the near-field sound holography technology and fault frequency, a 2.5D sound

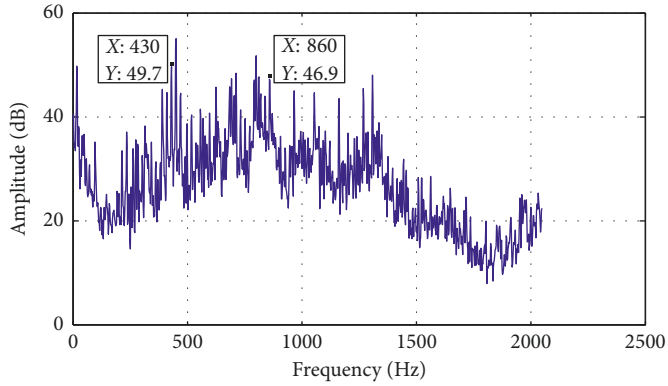

Figure 6: Spectrum analysis of reference source 3 under fault conditions.

field model is constructed for every test operating condition sample and one sound field model under normal and fault conditions is randomly selected, as shown in Figure 7.

The positions of bearing 1 and bearing 2 in the source images in Figures 7(a) and 7(b) can be basically identified. However, there is a certain gap compared with the intensity of the sound source near the rotor position. At the same time, due to the closer distance between the scanning equipment and one side of the test bench, a larger sound reflection is generated, which leads to more large amplitude interference noise sources in the source images in Figures 7(a) and 7(b). The sound images in Figures 7(c) and 7(d) of the holographic surface are the results after radiating a certain distance from the sound source space, and the influence on the strong interference source on the hemline is gradually reduced, and the sound pressure distribution at each sound source location is relatively obvious under normal and fault conditions. The distribution regularity of sound pressure is relatively poor in difference acoustic images in Figures 7(e) and 7(f), but the variation and difference of sound pressure distribution near the bearing and rotor position can also be identified. The overall comparison of the 2.5D acoustic field model under normal and fault conditions shows the key component bearing 2 has certain changes in source image, holographic image, and difference acoustic image. The difference in different acoustic images means the increasing effective fault information, which provides a basis for improving the diagnosis robustness.

The 2.5D acoustic field model integrates not only more effective fault information but also a lot of redundant and invalid information. Based on the idea of information fusion, the diagnostic robustness can be only improved effectively when the amount of effective information is greater than that of the redundant information. The Gabor wavelet texture features of 80 dimensions are directly extracted from every acoustic image in the 2.5D sound field model, and the texture features of 240 dimensions are sequentially arranged on three sides. Then, the significance of Gabor wavelet texture features of each dimension is analyzed through the random forest algorithm, as shown in Figure 8.

As is seen in Figure 8, the number of important features and proportion of importance of the source image are generally superior. However, the sum of the number of high proportion features with the proportion more than 0.05 in holographic sound image and difference sound image is more than that of the source image, and even the feature with the maximum significance up to 0.149 appears in the image features of the holographic surface. This means that the feature information of holographic image and difference sound image is an important value to the diagnostic classification. By analyzing the importance of texture features, the effective and important texture features are selected, some redundant and invalid texture features are discarded, and then, diagnostic robustness is improved with feature dimension reduction.

For the five sets of samples which have been randomly divided, the 2D NAH-based diagnosis technique based on single source image texture feature is adopted for diagnosis analysis and the average recognition effect is 0.844.

When using the 2.5D NAH-based diagnostic technique based on the spatial characteristics of 2.5D sound field proposed in this paper, the random forest algorithm is used to sort the importance of the features, and the feature combination is selected according to different proportions in order to build an effective sound field feature model. It means that the 240 Gabor wavelet features are ranked based on importance, and different 2.5D sound field feature models can be constructed by different numbers of the 240 features. For example, 10% denotes that the top 24 Gabor wavelet features are selected to build a feature model for diagnosis and analysis. The average identification rate of the five sets of samples varies with the proportion of the number of features, as shown in Figure 9. The recognition rate exceeds 0.9 when the feature ratio is 3%, 5%, 7%, 10%, 15%, 20%, and 25%, and especially, when the feature quantitative ratio is 20%, the highest recognition rate reaches 0.955.

By comparing the diagnostic results of sound image and 2.5D sound field and analyzing the changes of recognition rate with the percentage of feature number in Figure 9, the following can be obtained:

(1) The highest recognition rate of the 2.5D sound field diagnosis technology based on the spatial characteristics of the 2.5D sound field is 11.1% higher than that based on the 2D source image, indicating that the new 2.5D NAH-based diagnosis technique

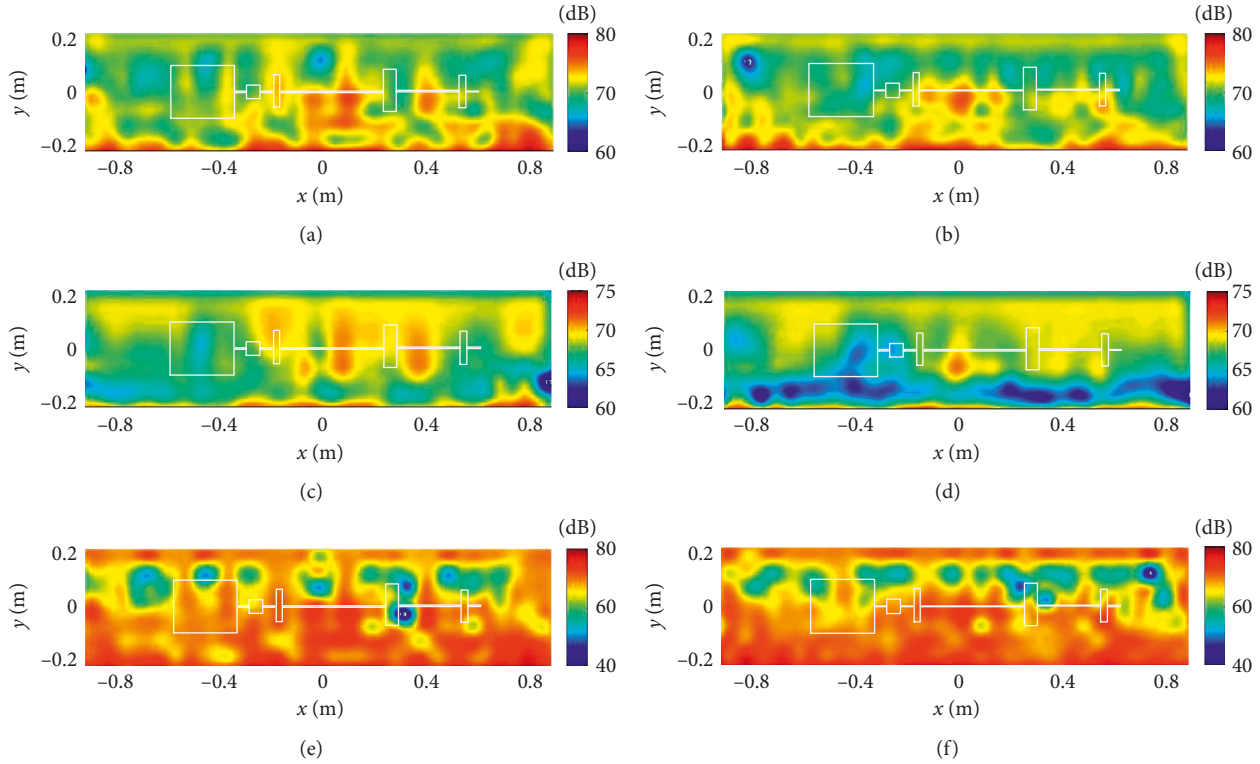

Figure 7: The 2.5D sound field model obtained under experimental conditions. (a) Normal state source image; (b) fault state source image; (c) normal state holographic sound image; (d) fault state holographic sound image; (e) normal state difference sound image; (f) fault state difference sound image.

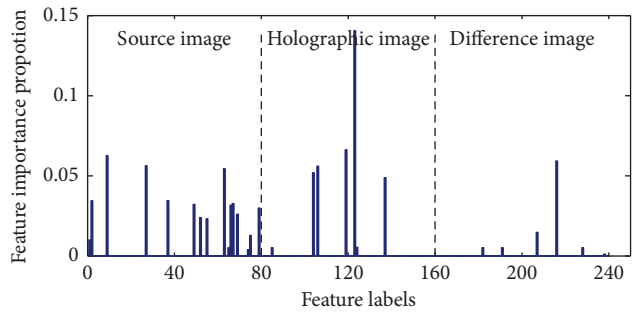

Figure 8: Feature importance of 2.5D sound field model.

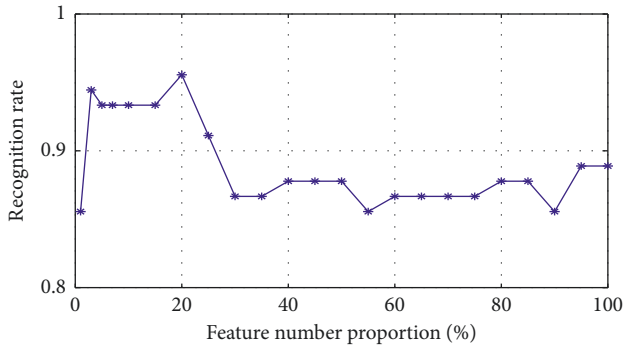

Figure 9: The recognition rates varying the percentile of texture features selected.

within integrating spatial variation information of normal sound field which is proposed in this paper has richer diagnostic information and better diagnostic efficiency.

(2) When all 240 dimensional texture features are used to build the 2.5D acoustic field model, the recognition rate is 0.888, which is 4.44% higher than the recognition rate of the sound image diagnostic technology based on 80 dimensional texture features of a single source. However, the amount of feature dimension increases by two times, indicating that the effective diagnostic information increases while the redundant information also increases.

(3) The recognition rate fluctuates with the proportion of number of valid texture features. It shows that the effective information and the redundant information increase alternately, and the best diagnosis effect can be obtained only when the two information reaches a certain balance.

4. Conclusions

The new 2.5D sound field diagnosis technique further improves the NAH-based diagnosis technology. By using the source acoustic image, holographic acoustic image, and the difference acoustic image of the two, a 2.5D acoustic field model is constructed, which integrates the acoustic field variation information at different spatial locations. Then, the spatial feature dimension is reduced based on the random forest feature selection algorithm, effective feature information is retained, redundant information is reduced, and diagnostic robustness is improved. The experimental results of the bearing show that the 2.5D sound field diagnosis technique is effective and feasible and has some advantages over the original 2D NAH-based diagnosis technology. By using the spatial variation information of sound field for diagnosis and analysis, the NAH-based diagnosis technology with array measurement is expanded and improved, further enriching the ABD technology.

Data Availability

The Mat data used to support the findings of this study were supplied by Junjian Hou under license and so cannot be made freely available. Requests for access to these data should be made to Junjian Hou at houjunjian@zzuli.edu.cn.

Conflicts of Interest

The authors declare that they have no conflicts of interest.

Acknowledgments

This work was supported by the National Natural Science Foundation of China (Grant no. 51505433); Scientific and Technological Research Projects of Henan (Grant no. 172102210058); Ph.D. Early Development Program of Zhengzhou University of Light Industry (Grant no. 2014BSJJ015); and the Plan of Key Research Projects of Higher Education of Henan Province (Grant no. 16A460028).

References

[1] H. Tang, J. Chen, and G. Dong, "Dynamic linear models-based time series decomposition and its application on bearing fault diagnosis," *Journal of Vibration and Control*, vol. 21, no. 5, pp. 975–988, 2013.

[2] M. K. Pradhan and P. Gupta, "Fault detection using vibration signal analysis of rolling element bearing in time domain using an innovative time scalar indicator," *International Journal of Manufacturing Research*, vol. 12, no. 3, pp. 305–317, 2017.

[3] Q. Miao, D. Wang, and H.-Z. Huang, "Identification of characteristic components in frequency domain from signal singularities," *Review of Scientific Instruments*, vol. 81, no. 3, article 035113, 2010.

[4] C. Shen, F. Liu, D. Wang, A. Zhang, F. Kong, and P. Tse, "A Doppler transient model based on the laplace wavelet and spectrum correlation assessment for locomotive bearing fault diagnosis," *Sensors*, vol. 13, no. 11, pp. 15726–15746, 2013.

[5] R. B. Randall, "A history of cepstrum analysis and its application to mechanical problems," *Mechanical Systems and Signal Processing*, vol. 97, pp. 3–19, 2017.

[6] X.-Y. Zhong, C.-H. Zhao, B.-J. Chen, and L.-C. Zeng, "Bearing fault diagnosis method based on morphological filtering, time-delayed autocorrelation and time-frequency slice analysis," *Zhendong yu Chongji/Journal of Vibration and Shock*, vol. 33, pp. 11–16, 2014.

[7] D. P. Jena and S. N. Panigrahi, "Automatic gear and bearing fault localization using vibration and acoustic signals," *Applied Acoustics*, vol. 98, pp. 20–33, 2015.

[8] N. H. Chandra and A. S. Sekhar, "Fault detection in rotor bearing systems using time frequency techniques," *Mechanical Systems and Signal Processing*, vol. 72-73, no. 73, pp. 105–133, 2016.

[9] Q. He, "Time-frequency manifold for nonlinear feature extraction in machinery fault diagnosis," *Mechanical Systems and Signal Processing*, vol. 35, no. 1-2, pp. 200–218, 2013.

[10] L. Xiang, A. Hu, L. Hou, Y. Xiong, and J. Xing, "Nonlinear coupled dynamics of an asymmetric double-disc rotor-bearing system under rub-impact and oil-film forces," *Applied Mathematical Modelling*, vol. 40, no. 7-8, pp. 4505–4523, 2016.

[11] P. Henriquez, J. B. Alonso, M. A. Ferrer, and C. M. Travieso, "Review of automatic fault diagnosis systems using audio and vibration signals," *IEEE Transactions on Systems, Man, and Cybernetics: Systems*, vol. 44, no. 5, pp. 642–652, 2014.

[12] F. Elasha, M. Greaves, D. Mba, and D. Fang, "A comparative study of the effectiveness of vibration and acoustic emission in diagnosing a defective bearing in a planetry gearbox," *Applied Acoustics*, vol. 115, pp. 181–195, 2017.

[13] M. A. A. Elmaleeh, N. Saad, N. Ahmed, and M. Awan, "Online fault detection & diagnosis of rotating machines using acoustic emission monitoring techniques," in *Proceedings of International Conference on Intelligent & Advanced Systems IEEE*, Kuala Lumpur, Malaysia, November 2008.

[14] W. Li, Y. P. Tsai, and C. L. Chiu, "The experimental study of the expert system for diagnosing unbalances by ANN and acoustic signals," *Journal of Sound and Vibration*, vol. 272, no. 1-2, pp. 69–83, 2004.

[15] U. Benko, J. Petrovcic, Đ. Juricic, J. Tavcar, and J. Rejec, "An approach to fault diagnosis of vacuum cleaner motors based on sound analysis," *Mechanical Systems and Signal Processing*, vol. 19, no. 2, pp. 427–445, 2005.

[16] F. Al Thobiani, F. Gu, and A. Ball, "The monitoring of cavitation in centrifugal pumps based on the analysis of vibro-acoustic measurements," in *Proceedings of Seventh International Conference on Condition Monitoring and Machinery Failure Prevention Technologies*, vol. 53, pp. 201–253, Stratford-upon-Avon, UK, June 2010.

[17] N. Baydar and A. Ball, "Detection of gear failures via vibration and acoustic signals using wavelet transform," *Mechanical Systems and Signal Processing*, vol. 17, no. 4, pp. 787–804, 2003.

[18] W. Lu, W. Jiang, H. Wu, and J. Hou, "A fault diagnosis scheme of rolling element bearing based on near-field acoustic

holography and gray level co-occurrence matrix," *Journal of Sound and Vibration*, vol. 331, no. 15, pp. 3663–3674, 2012.

[19] J. Hou, W. Jiang, and W. Lu, "Application of a near-field acoustic holography-based diagnosis technique in gearbox fault diagnosis," *Journal of Vibration and Control*, vol. 19, no. 1, pp. 3–13, 2011.

[20] W. Lu, W. Jiang, G. Yuan, and L. Yan, "A gearbox fault diagnosis scheme based on near-field acoustic holography and spatial distribution features of sound field," *Journal of Sound and Vibration*, vol. 332, no. 10, pp. 2593–2610, 2013.

[21] Y. B. Yang, X. Liang, H.-H. Hung, and Y. Wu, "Comparative study of 2D and 2.5D responses of long underground tunnels to moving train loads," *Soil Dynamics and Earthquake Engineering*, vol. 97, pp. 86–100, 2017.

[22] K. C. Lin, H. H. Hung, J. P. Yang, and Y. B. Yang, "Seismic analysis of underground tunnels by the 2.5D finite/infinite element approach," *Soil Dynamics and Earthquake Engineering*, vol. 85, pp. 31–43, 2016.

[23] J. Yin, L. Liu, H. Li, and Q. Liu, "The infrared moving object detection and security detection related algorithms based on W4 and frame difference," *Infrared Physics & Technology*, vol. 77, pp. 302–315, 2016.

[24] Y. Luo, H. Zhou, Q. Tan, X. Chen, and M. Yun, "Key frame extraction of surveillance video based on moving object detection and image similarity," *Pattern Recognition and Image Analysis*, vol. 28, no. 2, pp. 225–231, 2018.

[25] J. D. Maynard, E. G. Williams, and Y. Lee, "Nearfield acoustic holography: I. Theory of generalized holography and the development of NAH," *Journal of Acoustical Society of America*, vol. 78, no. 4, pp. 1395–1413, 1985.

[26] W.-B. Lu, W.-K. Jiang, and J.-J. Hou, "Approach of mechanical fault diagnosis based on textural features of beamforming acoustic images," *Zhendong Gongcheng Xuebao/ Journal of Vibration Engineering*, vol. 24, pp. 428–434, 2011.

[27] Y. Tong, Y. Wang, Z. Zhu, and Q. Ji, "Robust facial feature tracking under varying face pose and facial expression," *Pattern Recognition*, vol. 40, no. 11, pp. 3195–3208, 2007.

[28] K. B. Raja, M. Madheswaran, and K. Thyagarajah, "Texture pattern analysis of kidney tissues for disorder identification and classification using dominant gabor wavelet," *Machine Vision and Applications*, vol. 21, no. 3, pp. 287–300, 2010.

[29] Q. Zhou, H. Zhou, Q. Zhou, F. Yang, and L. Luo, "Structure damage detection based on random forest recursive feature elimination," *Mechanical Systems and Signal Processing*, vol. 46, no. 1, pp. 82–90, 2014.

[30] Y. Li, Y. Yang, X. Wang, B. Liu, and X. Liang, "Early fault diagnosis of rolling bearings based on hierarchical symbol dynamic entropy and binary tree support vector machine," *Journal of Sound and Vibration*, vol. 428, pp. 72–86, 2018.